Published in final edited form as:

Mol Pharm. 2017 August 07; 14(8): 2793–2804. doi:10.1021/acs.molpharmaceut.7b00321.

RGD-Modified Albumin Nanoconjugates for Targeted Delivery of a Porphyrin Photosensitizer

Fang Li[1,2], **Yan Zhao**[1], **Chengqiong Mao**[1], **Yi Kong**[3], and **Xin Ming**[1,*]

[1]Department of Cancer Biology and Comprehensive Cancer Center, Wake Forest University School of Medicine, Winston-Salem, NC 27157, USA

[2]School of Pharmacy, Jiangsu Vocational College of Medicine, Yancheng 224005, China

[3]School of Life Science and Technology, China Pharmaceutical University, Nanjing 210009, China

Abstract

Advances in photodynamic therapy of cancer have been restrained by lack of cancer specificity and side effects to normal tissues. Molecularly targeted photodynamic therapy can achieve higher cancer specificity by combination of active cancer targeting and localized laser activation. We aimed to use albumin as a carrier to prepare targeted nanoconjugates that are selective to cancer cells and smaller than conventional nanoparticles for superior tumor penetration. IRDye® 700DX (IR700), a porphyrin photosensitizer, was covalently conjugated to human serum albumin that was also linked with tumor-targeting RGD peptides. With multiple IR700 and RGD molecules in a single albumin molecule, the resultant nanoconjugates demonstrated monodispersed and uniform size distribution with a diameter of 10.9 nm. These targeted nanoconjugates showed 121-fold increase in cellular delivery of IR700 into TOV21G ovarian cancer cells compared to control nanoconjugates. Mechanistic studies revealed that the integrin specific cellular delivery was achieved through dynamin-mediated caveolae-dependent endocytosis pathways. They produced massive cell killing in TOV21G cells at low nanomolar concentrations upon light irradiation, while NIH/3T3 cells that do not express integrin $\alpha v\beta 3$ were not affected. Because of their small size, targeted albumin nanoconjugates could penetrate tumor spheroids of SKOV-3 ovarian cancer cells and produced strong phototoxicity in this 3-D model. Owing to their cancer-specific delivery and small size, these targeted nanoconjugates may become an effective drug delivery system for enabling molecularly targeted photodynamic therapy of cancer.

Graphical Abstract

*Corresponding author: Dr. Xin Ming, xming@wakehealth.edu, Phone number: 1-336-716-8440.

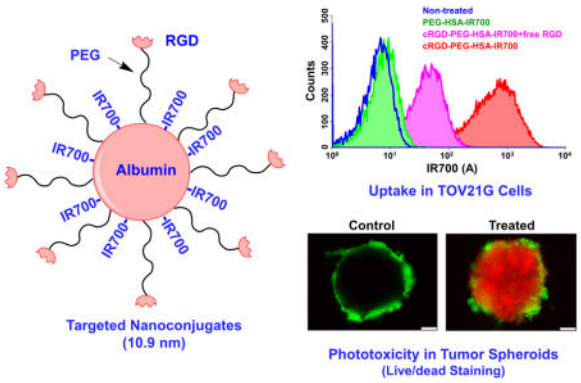

Keywords

Photodynamic Therapy; RGD peptide; Integrins; Nanoconjugates; Nanoparticles; Targeted delivery

Introduction

Photodynamic therapy (PDT) is a clinically approved cancer therapy. After a photosensitizer (PS) accumulates in tumors, irradiation with specific wavelengths of light triggers energy transfer cascades that ultimately produce cytotoxic singlet oxygen and/or free radical, capable of rendering cancer cell death.[1, 2] Local PDT damage is accompanied by damage to the microvasculature, which restricts oxygen and nutrient supply,[1, 3, 4] and by induction of local and systemic immunity, which enables cancer suppression in metastatic sites.[5–7] Since the first clinical study in1978, six PDT drugs have been approved for cancer treatment and another six drug candidates are in clinical trials.[8] Despite many merits as cancer therapy, PDT is not a mainstream cancer therapy. One key hurdle for wider application of PDT is inadequate tumor specificity of phototoxicity. Thus, the patients' skin may become sensitive to sunlight following systemic administration of PSs, and the normal tissues overlaying or adjacent to the tumor may be severely damaged, reducing the maximum tolerated dose of PS and limiting the efficacy. Therefore, novel strategies are required to further enhance cancer specificity to overcome intrinsic limitations of PDT.[9]

Active targeting approaches can be applied to deliver PSs to reduce toxicity of PDT in normal tissues. Thus, in the process of photoimmunotherapy, PS is conjugated to cancer-selective antibodies and is activated with a light at the tumor site to induce rapid cancer cell death. Photoimmunotherapy achieves higher cancer specificity by combination of antibody-based cancer targeting and localized laser activation. Thus, cancer selectivity can be achieved with limiting phototoxicity to cancer cells by targeted delivery of the PSs, thereby increasing their tolerated dose.[10] A phase I human study of photoimmunotherapy using cetuximab-IR700, targeting tumoral epidermal growth factor receptor,[11] is currently ongoing for the treatment of head and neck cancers (NCT02422979).

Besides antibodies, albumin is another protein that has been successfully used as a drug carrier.[12] Albumin, a biocompatible, biodegradable, and water-soluble globular protein,

possesses high affinity with secreted protein acidic and rich in cysteine (SPARC) which is highly expressed in most cancers.[13–15] Thus, some albumin-based systems delivered drugs to tumors through this SPARC-dependent pathway.[13, 16] Besides this endogenous mechanism, other strategies, including ligand modification, have been used to expand tumor targeting capability of albumin-based delivery system.[17–22]

Integrins are main targets for cancer-selective delivery of chemotherapy agents and therapeutic macromolecules.[23–25] Integrins consist of α and β subunits which form 24 integrin heterodimers in mammals.[26] As the main transmembrane cell adhesion and signaling receptor proteins, about half of integrin heterodimers connect the cytoskeleton with the extracellular matrix (ECM) via binding to Arginine-Glycine-Aspartic Acid (RGD) sequence.[26, 27] Integrins play pivotal roles in cancer progression, such as proliferation, invasion and metastasis, through binding to ECM components.[28] Some integrins, including αvβ3 and αvβ5, are overexpressed in neovasculature and some tumors including ovarian cancer (OvCa).[29–31] Since the RGD motif is recognized by half integrins, RGD-containing peptides have been widely used as targeting ligand for cancer diagnosis[32–35] and therapy[36–40].

Besides cancer cell targeting, tumor penetration of drugs is also crucial for cancer therapy. Tumor only can be eradicated without recurrences when all the tumor cells are treated by anticancer drugs at effective doses.[41] Size plays a substantial role on the biodistribution and tumor penetration of a drug delivery system.[42] Nanoparticles (NPs) for cancer therapy are typically larger than 80 nm, and thus can utilize the enhanced permeability and retention (EPR) effect for greater tumor delivery.[43] However, tumors are highly heterogeneous and blood vessels in different tumor sites show varied leakage.[44] Thus, conventional NPs may have poor delivery in less leaky sites, leading to incomplete eradication of the tumor. In addition, large tumors develop high interstitial fluid pressure that prevents tumor penetration of NPs through convection.[45, 46] Diffusion is the main motion for drugs to penetrate tumors, and it favors smaller particles.[44] Therefore, reducing size of drug carriers is an effective approach to enhance tumor penetration of drugs.

Our long-term goal was to use small targeted NPs for treating OvCa, and the purpose of this present study was to construct targeted nanoconjugates of PSs that are selective to OvCa cells and are smaller than 20nm for superior tumor penetration. OvCa is a leading cause of death from cancer in women with a projected 14,240 deaths in US in 2016.[47] Known as a “silent killer”, OvCa is generally diagnosed at advanced stages when patients present with numerous metastatic nodules studding the peritoneal cavity.[48] The residual micrometastases that are responsible for recurrence of OvCa are ideal targets for PDT because the residual nodules are less than 5 mm in depth and primarily disseminated within the peritoneal cavity after surgical debulking.[1, 49] In a PDT procedure, a laser can irradiate the micrometastases of OvCa intraperitoneally by means of flexible fiber-optic devices after systemic administration of PSs. Expression of integrin αvβ3 was detected in two third of human OvCa tissue samples in two studies,[50, 51] indicating integrin αvβ3 is a promising marker for OvCa targeted drug delivery. In this study, we chose albumin with a diameter of 7 nm as a core molecule to carry a porphyrin photosensitizer, IRDye 700DX (IR700). To achieve selectivity towards OvCa, RGD peptides were functionalized to the surface of albumin conjugates via

polyethylene glycol (PEG). The targeted nanoconjugates were characterized in size, absorption spectra, and photoactivity. We then examined cellular uptake and phototoxicity of the resultant nanoconjugates in TOV21G cells, an integrin αvβ3-expressing OvCa cell line, and further studied their delivery and phototoxicity in 3-D tumor spheroids of SKOV3 cells.

Materials and Methods

Synthesis of cRGD-PEG-HSA-IR700 nanoconjugates

The cRGD-PEG-HSA-IR700 nanoconjugates were synthesized according to procedures reported previously.[52] In brief, human serum albumin (HSA, Sigma-Aldrich, St. Louis, MO, USA) was conjugated with IR700-NHS (LI-COR Biosciences, Nebraska, USA) at a 1:5 molar ratio of HSA to IR700 in PBS buffer (pH 7.5) for 1 h at room temperature. In the meantime, the targeting peptide cyclo[RGDfK(Ac-SCH2CO)] (Peptides International, Inc., Louisville, Kentucky, USA) was activated with 50 mM hydroxylamine for 1 h at room temperature. HSA-IR700 and RGD-SH were added to Mal-PEG-SCM (MW 3.4K, Creative PEGWorks, Winston-Salem, North Carolina, USA) at a 1:20:40 molar ratio (HSA to PEG to RGD) and reacted in PBS-EDTA buffer (pH 7.2) for 2 h at room temperature. Finally, the resulting product was purified using a Zeba™ spin desalting column (40K MWCO, Thermo Fisher Scientific, Rockford, Illinois, USA). PEG-HSA-IR700 nanoconjugates used as non-targeting control were prepared by reacting HSA-IR700 with mPEG-SCM (Creative PEGWorks) at a 1:20 molar ratio.

Characterization of cRGD-PEG-HSA-IR700 nanoconjugates

The final nanoconjugates were analyzed using size-exclusion chromatography (SEC). Samples (50 μL) containing cRGD-PEG-HSA-IR700, HSA or free IR700 were separately injected into an UltiMate™ 3000 UHPLC system (Thermo Scientific, Dionex, Sunnyvale, CA, USA) equipped with an AdvanceBio SEC-300A column (Agilent Technologies, Inc., Santa Clara, CA, USA). All the samples were monitored at the absorbance of 689 nm and 280 nm. In addition, UV/Vis spectra were recorded over a wavelength range of 230–750 nm on a CYTATION 5 imaging reader (BioTeK™ Instruments, Inc., Winooski, VT, USA).

To examine the morphology of the nanoconjugates, the cRGD-PEG-HSA-IR700 nanoconjugates were diluted with deionized water and one droplet was placed on 200 mesh carbon-coated copper grid (Ted Pella, Inc., Redding, CA, USA) according to a method described previously.[53] After staining with phosphotungstic acid aqueous solution (2%) for 30 sec, the nanoconjugates were imaged using a transmission electron microscope operating at 80 kV (FEI Tecnai™, Hillsboro, OR, USA). The particle size of cRGD-PEG-HSA-IR700 was determined using dynamic light scattering (DLS) on a Zetasizer Nano ZS (Malvern Instruments, Westborough, MA, USA) with free albumin solution used as control.

To assess light induced singlet oxygen generation (SOG) of the nanoconjugates, the singlet oxygen sensor green (SOSG, Life Technologies, Carlsbad, CA, USA) and cRGD-PEG-HSA-IR700 was co-diluted with PBS and achieved final concentrations of 2 μM and 1 μM, respectively. The solution was then irradiated with a 660 nm LED light at the intensity of 3.5 mW/cm^2 for 0, 1, 3, 5, 10, 20 and 30 min, respectively. Then, the fluorescence intensity of

the solution was determined on a CYTATION 5 imaging reader (BioTeK) with the excitation wavelength of 504 nm and the emission wavelength of 525 nm. The fluorescence intensity of SOSG mixed with PBS, free IR700, or PEG-HSA-IR700 was also measured.

Cell culture

OvCa cell line TOV21G and mouse fibroblast NIH/3T3 were cultured in Dulbecco's Modified Eagle's Medium supplemented with 10% (v/v) FBS and 100 U/mL penicillin/streptomycin at 37°C with 5% CO_2. Another OvCa cell line SKOV-3 was cultured in McCoy's 5A medium supplemented with 10% FBS, and 100 U/mL penicillin/streptomycin.

Intracellular uptake and distribution

To study the intracellular uptake behavior of the targeted nanoconjugates, TOV21G and NIH/3T3 cells were seeded in a glass bottom chamber, respectively, and were cultured overnight. The cells were separately treated with PEG-HSA-IR700 and cRGD-PEG-HSA-IR700 in the absence and presence of 10 μM free cRGDyK for another 4 h. All the doses contained 100 nM of IR700 equivalent. The cells were then washed with cold PBS thrice, stained with Hoechst 33342 (Life technologies), and visualized with Olympus FV1200 confocal microscopy (Olympus, Tokyo, Japan). Co-localization of the cRGD-PEG-HSA-IR700 nanoconjugates with Lysotracker Green DND-26 (Life technologies) was also performed using confocal microscopy.

Flow cytometry was used to quantify the cellular uptake. TOV21G cells were cultured in 24-well plate overnight, and were then incubated with PEG-HSA-IR700 and cRGD-PEG-HSA-IR700 nanoconjugates in the absence and presence of free cRGDyK peptide (10 μM) for 4 h. The cells were washed with cold PBS thrice, trypsinized and analyzed using BD LSRFortessa X-20 flow cytometer (BD, Franklin Lakes, NJ, USA).

To examine the uptake mechanism of cRGD-PEG-HSA-IR700, the following endocytosis inhibitors were used: 5 μM cytochalasin D (actin polymerization inhibitor[54]), 40 μM chlorpromazine (clathrin-mediated endocytosis inhibitor[55]), 7.5 mM methyl-β-cyclodextrin (caveolae-dependent endocytosis inhibitor[56]), and 300μM Amiloride (micropinocytosis inhibitor[57]). After incubating TOV21G cells with the inhibitors for 30 min, the targeted nanoconjugates was added to the inhibitor-containing media. After 4-hr incubation, the cells were washed, trypsinized and analyzed with flow cytometry.

Dynamin is a small GTPase that mediates pinching off membrane vesicles in both clathrin- and caveolae-dependent endocytotic pathways.[58] The role of dynamin in RGD-targeted nanoconjugate uptake was examined as described previously.[59, 60] Briefly, TOV21G cells were transfecting cells with a plasmid coding for a chimeric protein comprised of a dominant negative form of dynamin and eGFP (pDN-dynamin-eGFP). After transfection, intracellular uptake of the cRGD-PEG-HSA-IR700 nanoconjugates was quantified with flow cytometry.

Phototoxicity study

The phototoxicity of the nanoconjugates was examined with live/dead staining. After culture overnight, TOV21G cells were treated with the nanoconjugates containing 100 nM IR700 for 16 h, then irradiated using the 660 nm LED light (3.5mW/cm^2) for 20 min after replacing the drug-containing medium with fresh medium. After 6 h, the cells were co-stained with Calcein AM (2 μM) and PI (5 μg/mL) at room temperature for 30 min, rinsed with PBS, and then imaged using an Olympus IX83 inverted microscope.

The phototoxicity of the nanoconjugates was also determined using Alamar Blue assay according to a method described previously.[52, 53] Briefly, three thousand per well of TOV21G cells were seeded in 96-well plates and cultured overnight. Subsequently, the cells were separately incubated with different concentrations of free IR700, PEG-HSA-IR700 and cRGD-PEG-HSA-IR700 nanoconjugates overnight. Then, drug-containing medium was replaced with fresh medium, and cells were irradiated with the 660 nm LED light (3.5 mW/cm^2) for 20 min. After 24 h, Alamar Blue reagent (Life Technologies) was added and incubated for 2 h. The fluorescence of the samples was then measured on a CYTATION 5 imaging reader (BioTeK) set at 540 nm excitation wavelength and 590 nm emission wavelength. NIH/3T3 cells were used as a control cell line as they do not express integrin $\alpha v\beta 3$.

To study the effect of light dose on the photokilling of cRGD-PEG-HSA-IR700, TOV21G cells were incubated with cRGD-PEG-HSA-IR700 overnight, and irradiated using the 660 nm LED light (3.5 mW/cm^2) for 0, 5, 10 and 20 min, respectively, or exposed to room lights for 20 min. After 24 h, cell viability was determined using an Alamar Blue assay.

Intracellular singlet oxygen observation with photo-irradiation

After incubated with cRGD-PEG-HSA-IR700 (100 nM IR700) overnight, 10 μM CM-H2DCFDA (Life Technologies) was added into the TOV21G cells and incubated for 30 min. Then the singlet oxygen indicator was replaced with fresh medium and the cells were irradiated with the 660 nm LED light (3.5mW/cm^2) for 20 min. The intracellular ROS was observed and captured by Olympus IX83 inverted fluorescence microscopy.

Apoptosis mediated by cRGD-PEG-HSA-IR700

After incubation with cRGD-PEG-HSA-IR700 (100 nM IR700) overnight, TOV21G cells were irradiated using the 660 nm LED light (3.5 mW/cm^2) for 20 min after the dose solution was replaced with fresh medium. After 2 or 24 h, the cells were trypsinized, washed once, and stained with FITC-labelled Annexin V and PI (Life Technologies). The fluorescence of FITC and PI was detected with BD FACS Canto II flow cytometer (BD, Franklin Lakes, NJ, USA).

Penetration and phototoxicity of cRGD-PEG-HSA-IR700 in SKOV-3 spheroids

SKOV-3 spheroids were grown to study the penetration of nanoconjugates in a 3D tumor model according to a method described previously.[52] Briefly, 5×10^3 of SKOV-3 cells in 200 μL medium per well were seeded into ultra-low attachment 96-well round bottom plates (Thermo Scientific), centrifuged at 200 × g for 3 min and cultured for 7 days. To examine

the penetration of the nanoconjugates, free IR700 and cRGD-PEG-HSA-IR700, both containing 400 nM IR700, were given to the spheroids and treated for 4 h. Subsequently, the spheroids were washed thrice with fresh medium and imaged using an Olympus FV1200 confocal microscope.

To evaluate the phototoxicity, SKOV-3 spheroids were treated with PEG-HSA-IR700 and cRGD-PEG-HSA-IR700 (1 μM of IR700 equivalent) overnight. The spheroids were then rinsed with fresh medium and irradiated with the 660 nm LED light (3.5 mW/cm^2) for 30 min. After 24 h, Calcein AM/PI solution was added and incubated at 37°C for 30 min. The spheroids were washed thrice with fresh medium, and imaged using an Olympus IX83 inverted microscope. Meanwhile, the growth of spheroids was monitored using a CYTATION 5 imaging reader (BioTeK) over the following 12 days.

Statistical Analysis

Quantitative data were expressed as mean ± SD. Means were compared using Student's t test or one-way ANOVA followed by Tukey's post-hoc analysis. P values <0.05 were considered statistically significant.

Results

Synthesis and characterization of cRGD-PEG-HSA-IR700 nanoconjugates

The scheme for the preparation of the targeted nanoconjugates is shown in Fig. 1. First, the amino group of HSA reacted with NHS ester of IR700-NHS to form HSA-IR700. Approximately four IR700 molecules were covalently linked to HSA. In the meantime, hydroxylamine hydrochloride solution (pH 7.0) was added to cyclo[RGDfK(Ac-SCH2CO)] solution (5 mM) to activate thiol groups with constant shaking for 1 h. Subsequently, HSA-IR700 and RGD-SH were added to Mal-PEG-SCM at a 1:20:40 molar ratio (HSA to PEG to RGD) and reacted for 2 h at room temperature. The final product of cRGD-PEG-HSA-IR700 was purified by gel filtration using a Zeba™ spin desalting column.

The SEC-HPLC chromatograms of HSA, IR700 and the resultant nanoconjugates are shown in Fig. 2A. cRGD-PEG-HSA-IR700 eluted earlier than free IR700 and HSA (Fig. 2A) with the retention time of 8.07, 11.92 and 8.36 min, respectively. A strong peak appeared at 280 nm (Fig. 2A), while no absorption peaks were shown in the chromatogram of HSA at 689 nm (Fig. 2A). A strong peak appeared in the chromatograms of free IR700 with the similar retention time, as well as cRGD-PEG-HSA-IR700, which indicated that IR700 was successfully linked to the albumin.

The UV-Vis absorbance spectra of PBS, HSA, free IR700, and cRGD-PEG-HSA-IR700 is shown in Fig. 2B. Around 278 nm appeared a characteristic absorbance peak of HSA owing to the $\pi \rightarrow \pi^*$ transition of the aromatic amino acid residues including tyrosine, tryptophan, and phenylalanine. Four peaks were displayed in the spectrum of free IR700 around 260, 346, 620 and 689 nm, respectively. As shown in the spectrum of cRGD-PEG-HSA-IR700, there are one weak peak (around 267nm) and three strong peaks (349, 620 and 689 nm). The appearance of the characteristic absorption peaks of IR700, the weakening

effect of the first peak and the long shift of the left two peaks revealed the successful linkage between IR700 and HSA.

The morphology of the nanoconjugates is shown by the TEM (Fig. 2C), and the particle size was estimated about 10 nm. Similar results are seen in the DLS data (Fig. 2D). The particle size and PDI of HSA solution was 7.21 ± 0.25 nm and 0.224 ± 0.005, while the size of the targeted nanoconjugates increased to 10.90 ± 0.11 nm with the PDI of 0.218 ± 0.004.

SOG was determined using the SOSG probe. The fluorescence intensity of SOSG solutions before and after irradiation is shown in Fig 2E. A remarkable fluorescence increase was observed in all the IR700-containing groups, whereas the PBS group did not show obvious fluorescence change. The IR700 nanoconjugates demonstrated slow onset and generated less $^{1}O2$ than free IR700 in the first 10 min, but caught up after 20min irradiation. The results suggested that a type II mechanism is involved in the nanoconjugate-mediated PDT.

Intracellular uptake

We examined intracellular uptake of the nanoconjugates with fluorescence microscopy and flow cytometry. As shown in Fig. 3A, TOV21G cells treated with cRGD-PEG-HSA-IR700 demonstrated substantial IR700 fluorescence, whereas no signal was observed for PEG-HSA-IR700. Furthermore, cellular uptake of cRGD-PEG-HSA-IR700 was remarkably reduced by co-incubation with free RGD peptide, confirming that integrin-mediated endocytosis is the main uptake pathway for the cRGD-PEG-HSA-IR700 nanoconjugates. No IR700 signal was observed in NIH/3T3 cells after treated with PEG-HSA-IR700 or cRGD-PEG-HSA-IR700 (Fig 3B) because this cell line does not express integrin αvβ3. The flow cytometry results in Fig. 3C are consistent with the microscopy experiment. Compared to the control, only a slight fluorescence shift was observed in the PEG-HSA-IR700 treatment group, while a 121-fold increase was observed in the cRGD-PEG-HSA-IR700 treatment group compared to the control ($p < 0.001$, Fig. 3C). Moreover, dramatic reduction of the cRGD-PEG-HSA-IR700 uptake was also observed by the co-incubation with free RGD peptide (Fig. 3C).

Endocytosis mechanism

We examined the endocytosis mechanism of cRGD-PEG-HSA-IR700 with three methods. Firstly, the effects of endocytosis inhibitors on intracellular uptake rate of the targeted nanoconjugates were examined. Cytochalasin D blocks actin filament function, which is required for most pathways of endocytosis, while methyl-β-CD interferes selectively with caveolae/lipid raft-mediated endocytosis.[61] As shown in Fig. 4A, both cytochalasin D and methyl-β-CD inhibited the uptake of cRGD-PEG-HSA-IR700 significantly ($p < 0.001$), indicating that initial uptake of cRGD-PEG-HSA-IR700 involves caveolae. Chlorpromazine and amiloride inhibit clathrin-mediated endocytosis and macropinocytosis, respectively.[61] The lack of effects (Fig. 4A) suggests that clathrin coated vesicles are not involved in endocytosis of cRGD-PEG-HSA-IR700, nor is macropinocytosis. These results are consistent with literature on the endocytosis mechanism of integrin αvβ3.[62]

We confirmed the endocytosis mechanism using a molecular inhibitor of endocytosis. TOV21G cells were transfected with a dynamin DN plasmid to block dynamin-dependent

endocytosis pathways. These cells were then treated with PEG-HSA-IR700 and cRGD-PEG-HSA-IR700 and observed for the levels of the accumulated fluorescent conjugates. After transfection, TOV21G cells showed heterogeneous expression levels of mutant dynamin reflected by the eGFP expression profile in flow cytometry. In Figure 4B, the population of cells in Q1 and Q3 did not express DN-dynamin-eGFP and showed similar eGFP level as control cells, while the population in Q2 and Q4 showed positive expression of DN-dynamin-eGFP. High expression of the plasmid reduced the uptake of cRGD-PEG-HSA-IR700 to the level of PEG-HSA-IR700. This result indicated that the uptake of the targeted nanoconjugates depends on dynamin function, confirming the receptor-mediated endocytosis for cellular uptake of the targeted conjugates.

We then examined the intracellular location of the targeted nanoconjugates after they were delivered into cancer cells. The endo-lysosomes were stained in green with Lysotracker Green DND-26. The green signal of Lysotracker Green merged well with the signal of cRGD-PEG-HSA-IR700 (Fig. 4C), which indicated that cRGD-PEG-HSA-IR700 predominantly resided in the endo-lysosomes. Hence, after the uptake of cRGD-PEG-HSA-IR700 into TOV21G cells, the nanoconjugates enter endo-lysosomes of the cells.

Phototoxicity of targeted nanoconjugates

Phototoxicity of targeted nanoconjugates was examined with live/dead staining and Alamar blue assay. The live/dead staining results indicated that both control and targeted nanoconjugates did not cause photokilling without light irradiation because only live signals in green were observed for both treatments (Fig. 5B). After light treatment, only the cRGD-PEG-HSA-IR700 group showed strong dead signal in red (Fig. 5A), indicating the targeted nanoconjugates caused integrin-specific photokilling in TOV21G cells.

The results from Alamar blue assay suggested that free IR700 and PEG-HSA-IR700 were nontoxic to both TOV21G (Fig. 6A) and NIH/3T3 cells (Fig. 6B), while cRGD-PEG-HSA-IR700 significantly suppressed the growth of TOV21G cells (Fig. 6A), but not NIH/3T3 cells (Fig. 6B), confirming that photokilling by the targeted conjugates depends on integrin $\alpha v\beta 3$ specific cellular uptake.

We evaluated the effect of light dose on photokilling by cRGD-PEG-HSA-IR700 by measuring cytotoxicity of TOV21G cells after illuminated for various time periods. As shown in Fig. 6C, no cytotoxicity was observed without light irradiation, and photokilling was enhanced as irradiation time increased, indicating that the photokilling by cRGD-PEG-HSA-IR700 depends on light dose. To test whether our targeted nanoconjugates will cause the dark toxicity, we exposed TOV21G cells to room lights for 20 min after the cRGD-PEG-HSA-IR700 treatment. The results in Fig. 6C show no phototoxicity was observed from this treatment.

Intracellular singlet oxygen detection

The fluorescence of ROS generation within TOV21G cells is shown in Fig. 7A. No green fluorescence was found in all the groups without light irradiation, as well as the control group treated with light (Fig. 7A). Meanwhile, weak green signal was observed in the cells treated with PEG-HSA-IR700 followed by light irradiation due to the weak uptake of the

control nanoconjugates (Fig. 7A). Strong green fluorescence was observed in the cells treated with cRGD-PEG-HSA-IR700 followed by light irradiation (Fig. 7A), indicating that the generation of ROS caused the death of the targeted cancer cells.

Flow cytometric analysis of apoptosis caused by targeted PDT

To determine the mechanism of cRGD-PEG-HSA-IR700 mediated photokilling, TOV21G cells were harvested and stained with Annexin V-FITC/PI. Annexin V-FITC signal is observed in both early and late apoptosis, whereas PI signal is detected in late apoptosis and necrosis. As shown in Fig. 7B, after cultured for 2 h and 24 h post light, the ratio of live cells decreased from 91.5% for control cells to 88.3% and 35.6%, respectively. In contrast, the percentage of early apoptosis cells increased from 1.9% to 3.3% and 10.0%, respectively, and the percentage of late apoptotic cells increased from 6.4% to 8.3% and 53.7%, respectively (Fig. 7B). The results demonstrate that targeted PDT by cRGD-PEG-HSA-IR700 caused apoptosis of TOV21G cells.

Penetration and phototoxicity of cRGD-PEG-HSA-IR700 nanoconjugates in SKOV-3 spheroids

In order to achieve good therapeutic effect, effective penetration of drug molecules into the core of the tumor is crucial. Tumor spheroid is a reliable model for studying tumor penetration behavior of NPs due to their *in vivo*-like differentiation pattern.[53] TOV21 cells do not grow to tumor spheroids, and thus we used SKOV3 cells, another integrin αvβ3-expressing OvCa cell line, to examine the delivery and photokilling of our targeted nanoconjugates in 3D tumor model. We first confirmed the formation of spheroids by examining penetration of Doxil®, a liposomal formation of doxorubicin with a particle size of 80~85 nm, in this 3D model. The doxorubicin fluorescence was observed on the surface of SKOV3 spheroids (Fig. S1), indicating that the spheroids present a barrier for drug penetration. As shown in Fig. 8A, a strong IR700 fluorescence was observed in the cRGD-PEG-HSA-IR700 treatment group, whereas no signal was detected after treatment of free IR700, indicating that the targeted nanoconjugates may have an advantage in penetration of solid tumors *in vivo*.

Photokilling of nanoconjugates in SKOV-3 tumor spheroids was then evaluated using live/dead staining assay and microscopic observation. As shown in Fig. 8B, both the control spheroids and those treated with PEG-HSA-IR700 exhibited green live fluorescence, whereas the spheroids treated with cRGD-PEG-HSA-IR700 emitted strong red fluorescence, the dead cell signal, suggesting that cRGD-PEG-HSA-IR700 caused excellent photokilling in this 3D model. SKOV-3 spheroids were also used to examine *in vitro* tumor suppression by cRGD-PEG-HSA-IR700. As shown in Fig. 8C, the spheroids in control and PEG-HSA-IR700 groups grew gradually, whereas the growth of spheroids treated with cRGD-PEG-HSA-IR700 followed by light treatment was remarkably suppressed, confirming the superior photokilling by the targeted nanoconjugates.

Discussion

To overcome the various inherent disadvantages of conventional PDT, particularly, the toxicity in normal tissues, we aimed to construct monomolecular nanoconjugates that are small and highly cancer specific. Albumin, PEG, and RGD peptide were selected as the carrier molecules and targeting moiety, respectively, because all of them have demonstrated superior safety profiles in clinical applications. The resultant nanoconjugates showed narrow size distribution with a diameter of 10.9 nm, thus they are small enough to transport across most vasculatures in tumors. These smaller nanoconjugates are especially advantageous over conventional NPs due to their ability to deliver drugs to less leaky tumor sites, where relatively tight vasculatures and high interstitial fluid pressure prevent effective tumor penetration by larger NPs.[41]

The clinical significance of tumor targeting lies in the ability to accumulate a drug specifically in tumor cells and thereby to enhance therapeutic activity and minimize drug-related toxicity.[63] To achieve tumor targeting *in vivo*, multivalent display of the targeting moiety is often required because the endogenous ligands compete for binding to the target and the shear stress in the circulation drags the delivery system away from tumor sites.[63] The targeted nanoconjugates demonstrated 121-folded enhancement in receptor-specific uptake in OvCa cells compared to the non-targeted control nanoconjugates. This dramatically increased uptake is due to display of multivalent targeting ligands on the surface of the nanoconjugates developed here. In addition, the targeted nanoconjugates produced integrin specific phototoxicity to OvCa cells. These observations support the notion that displaying multivalent targeting peptides on the surface of a NP can dramatically enhance binding affinity of the ligands to the receptors.[64] Further, these data indicate that the enhanced receptor binding can lead to superior receptor-mediated cellular uptake and phototoxicity. Clinical practice of PDT is limited by the dark toxicity, in which the patients' skin may become sensitive to sunlight following systemic administration of PS.[1] Delivery with our targeted nanoconjugates may reduce the PS accumulation in non-tumor tissue including skins and prevent this side effect.

Integrin αvβ3 is expressed in tumors, as well as some normal tissues such as the liver and the kidney.[26] As our targeted nanoconjugates only produce cytotoxicity upon light irradiation (Figs 5 and 6), we can prevent off-target toxicity by localized light activation of the drug in tumor sites. Integrin αvβ3 is also present in the cells other than cancer cells in tumor sites. For example, endothelial cells in tumor neovasculatures express integrin αvβ3 at high levels.[26] Therefore, combining integrin targeting with PDT through our RGD-targeted nanoconjugates can damage tumor-associated vasculature to cut off blood supply thus contributing to tumor death indirectly. Integrins are also expressed in the immune cells including subsets of lymphocytes,[65] macrophages,[66] and dendritic cells[67] in tumor microenvironment. Numerous lines of evidence indicate that tumor microenvironment could alter myeloid cells (macrophages, dendritic cells, and granulocytes) and make them become potent immunosuppressive cells.[68, 69] Tumor-associated macrophages contribute to tumor survival and invasion by secreting cytokines and chemokines,[70] as well as maintaining pro-tumor inflammation.[68, 69] Tumor associated dendritic cells have serious functional deficits and cause cancer immunosuppression.[71] Therefore, both the macrophages and dendritic cells

in tumor microenvironment promote tumor progression. Our RGD-targeted nanoconjugates can deliver PSs to tumor-associated cells that express integrins, and targeted PDT can break symbiosis between cancer cells and tumor microenvironment and may further enhance antitumor effects *in vivo*.

In order to eradicate solid tumors completely, anticancer drugs need to penetrate tumors efficiently and reach a therapeutic concentration within all cancer cells.[41] Tumor spheroids resemble micrometastases, such as the residual micrometastases that are responsible for recurrence of OvCa, and therefore have been used to study tumor penetration of anticancer drugs.[72, 73] The targeted nanoconjugates developed here could penetrate 3-D tumor spheroids and enter most of cancer cells, whereas the conventional nanomedicine Doxil®, with the size over 80 nm, could only deliver to the cells on the outer layer of the tumor spheroids (Fig. S1). This result is consistent with our previous reports that nanoconjugates smaller than 20 nm showed superior penetration behavior into the tumor spheroid than conventional NPs typically larger than 80 nm.[52, 53] Besides size, other physicochemical properties, such as surface charge, also play a role in penetration behaviors of NPs in solid tumors.[73] In addition, there are additional biological barriers preventing drug delivery to tumor *in vivo* than that modeled by the tumor spheroids. For example, NPs need to cross blood vessels to reach cancer cells in tumors, however, this behavior cannot be studied in tumor spheroids due to the lack of blood vessels in this model. Therefore, substantial *in vivo* experimentation is warranted for further development of this targeted nanoconjugate system.

In conclusion, we successfully prepared multivalent nanoconjugates that are small, highly cancer specific, and non-toxic to normal cells. The targeted nanoconjugates demonstrated dramatic increases in integrin-specific cellular uptake, tumor spheroid penetration, and phototoxicity in cancer cells. Due to small size, excellent cellular delivery and good photoactivity, RGD-targeted nanoconjugates as described here may provide an effective tool for targeted PDT of OvCa.

Supplementary Material

Refer to Web version on PubMed Central for supplementary material.

Acknowledgments

This study was supported by NIH Grant R01CA194064 and Jiangsu Overseas Research & Training Program for University Prominent Professors. We gratefully acknowledge Dr. JoAnn Trejo (University of California at San Diego, USA) for providing the plasmid of DN-dynamin-eGFP.

Abbreviations

ECM	extracellular matrix
HSA	human serum albumin
IR700	IRDye® 700DX
NP	nanoparticle

OvCa	ovarian cancer
PDT	photodynamic therapy
PEG	polyethylene glycol
PI	propidium iodide
PS	photosensitizer
RGD	Arginine-Glycine-Aspartic Acid
ROS	reactive oxygen species

Uncategorized References

1. Agostinis P, Berg K, Cengel KA, Foster TH, Girotti AW, Gollnick SO, Hahn SM, Hamblin MR, Juzeniene A, Kessel D, Korbelik M, Moan J, Mroz P, Nowis D, Piette J, Wilson BC, Golab J. Photodynamic therapy of cancer: an update. CA: a cancer journal for clinicians. 2011; 61(4):250–81. [PubMed: 21617154]
2. Yoon I, Li JZ, Shim YK. Advance in photosensitizers and light delivery for photodynamic therapy. Clinical endoscopy. 2013; 46(1):7–23. [PubMed: 23423543]
3. Krammer B. Vascular effects of photodynamic therapy. Anticancer research. 2001; 21(6B):4271–7. [PubMed: 11908681]
4. Abels C. Targeting of the vascular system of solid tumours by photodynamic therapy (PDT). Photochemical & photobiological sciences : Official journal of the European Photochemistry Association and the European Society for Photobiology. 2004; 3(8):765–71.
5. St Denis TG, Aziz K, Waheed AA, Huang YY, Sharma SK, Mroz P, Hamblin MR. Combination approaches to potentiate immune response after photodynamic therapy for cancer. Photochemical & photobiological sciences : Official journal of the European Photochemistry Association and the European Society for Photobiology. 2011; 10(5):792–801.
6. Canti G, De Simone A, Korbelik M. Photodynamic therapy and the immune system in experimental oncology. Photochemical & photobiological sciences : Official journal of the European Photochemistry Association and the European Society for Photobiology. 2002; 1(1):79–80.
7. Castano AP, Mroz P, Hamblin MR. Photodynamic therapy and anti-tumour immunity. Nature reviews Cancer. 2006; 6(7):535–45. [PubMed: 16794636]
8. Yuan A, Wu J, Tang X, Zhao L, Xu F, Hu Y. Application of near-infrared dyes for tumor imaging, photothermal, and photodynamic therapies. Journal of pharmaceutical sciences. 2013; 102(1):6–28. [PubMed: 23132644]
9. Wang S, Huang P, Nie L, Xing R, Liu D, Wang Z, Lin J, Chen S, Niu G, Lu G, Chen X. Single continuous wave laser induced photodynamic/plasmonic photothermal therapy using photosensitizer-functionalized gold nanostars. Advanced materials. 2013; 25(22):3055–61. [PubMed: 23404693]
10. Mallidi S, Anbil S, Bulin AL, Obaid G, Ichikawa M, Hasan T. Beyond the Barriers of Light Penetration: Strategies, Perspectives and Possibilities for Photodynamic Therapy. Theranostics. 2016; 6(13):2458–2487. [PubMed: 27877247]
11. Mitsunaga M, Ogawa M, Kosaka N, Rosenblum LT, Choyke PL, Kobayashi H. Cancer cell-selective in vivo near infrared photoimmunotherapy targeting specific membrane molecules. Nature medicine. 2011; 17(12):1685–91.
12. Liu Z, Chen X. Simple bioconjugate chemistry serves great clinical advances: albumin as a versatile platform for diagnosis and precision therapy. Chemical Society reviews. 2016; 45(5): 1432–56. [PubMed: 26771036]
13. Li F, Zheng C, Xin J, Chen F, Ling H, Sun L, Webster TJ, Ming X, Liu J. Enhanced tumor delivery and antitumor response of doxorubicin-loaded albumin nanoparticles formulated based on a Schiff base. Int J Nanomedicine. 2016; 11:3875–90. [PubMed: 27574421]

14. Komiya K, Nakamura T, Nakashima C, Takahashi K, Umeguchi H, Watanabe N, Sato A, Takeda Y, Kimura S, Sueoka-Aragane N. SPARC is a possible predictive marker for albumin-bound paclitaxel in non-small-cell lung cancer. Oncotargets Ther. 2016; 9:6663–6668.
15. Vaz J, Ansari D, Sasor A, Andersson R. SPARC: A Potential Prognostic and Therapeutic Target in Pancreatic Cancer. Pancreas. 2015; 44(7):1024–35. [PubMed: 26335014]
16. Hoang B, Ernsting MJ, Roy A, Murakami M, Undzys E, Li SD. Docetaxel-carboxymethylcellulose nanoparticles target cells via a SPARC and albumin dependent mechanism. Biomaterials. 2015; 59:66–76. [PubMed: 25956852]
17. Gawde KA, Kesharwani P, Sau S, Sarkar FH, Padhye S, Kashaw SK, Iyer AK. Synthesis and characterization of folate decorated albumin bio-conjugate nanoparticles loaded with a synthetic curcumin difluorinated analogue. J Colloid Interface Sci. 2017; 496:290–299. [PubMed: 28236692]
18. Harada T, Nakamura Y, Sato K, Nagaya T, Okuyama S, Ogata F, Choyke PL, Kobayashi H. Near-infrared photoimmunotherapy with galactosyl serum albumin in a model of diffuse peritoneal disseminated ovarian cancer. Oncotarget. 2016; 7(48):79408–79416. [PubMed: 27765903]
19. Look J, Wilhelm N, von Briesen H, Noske N, Gunther C, Langer K, Gorjup E. Ligand-Modified Human Serum Albumin Nanoparticles for Enhanced Gene Delivery. Molecular pharmaceutics. 2015; 12(9):3202–13. [PubMed: 26218774]
20. Huang D, Chen YS, Rupenthal ID. Hyaluronic Acid Coated Albumin Nanoparticles for Targeted Peptide Delivery to the Retina. Molecular pharmaceutics. 2017; 14(2):533–545. [PubMed: 27997199]
21. Bansal R, Prakash J, de Ruijter M, Beljaars L, Poelstra K. Peptide-modified albumin carrier explored as a novel strategy for a cell-specific delivery of interferon gamma to treat liver fibrosis. Molecular pharmaceutics. 2011; 8(5):1899–909. [PubMed: 21800888]
22. Temming K, Meyer DL, Zabinski R, Senter PD, Poelstra K, Molema G, Kok RJ. Improved efficacy of alphavbeta3-targeted albumin conjugates by conjugation of a novel auristatin derivative. Molecular pharmaceutics. 2007; 4(5):686–94. [PubMed: 17683157]
23. Liu Z, Wang F, Chen X. Integrin targeted delivery of radiotherapeutics. Theranostics. 2011; 1:201–10. [PubMed: 21547160]
24. Juliano RL, Ming X, Nakagawa O, Xu R, Yoo H. Integrin targeted delivery of gene therapeutics. Theranostics. 2011; 1:211–9. [PubMed: 21547161]
25. Chen K, Chen X. Integrin targeted delivery of chemotherapeutics. Theranostics. 2011; 1:189–200. [PubMed: 21547159]
26. Hynes RO. Integrins: bidirectional, allosteric signaling machines. Cell. 2002; 110(6):673–87. [PubMed: 12297042]
27. Ulmasov B, Neuschwander-Tetri BA, Lai J, Monastyrskiy V, Bhat T, Yates MP, Oliva J, Prinsen MJ, Ruminski PG, Griggs DW. Inhibitors of Arg-Gly-Asp-Binding Integrins Reduce Development of Pancreatic Fibrosis in Mice. Cell Mol Gastroenterol Hepatol. 2016; 2(4):499–518. [PubMed: 28174730]
28. Marelli UK, Rechenmacher F, Sobahi TR, Mas-Moruno C, Kessler H. Tumor Targeting via Integrin Ligands. Frontiers in oncology. 2013; 3:222. [PubMed: 24010121]
29. Matsuura M, Suzuki T, Saito T. Osteopontin is a new target molecule for ovarian clear cell carcinoma therapy. Cancer Sci. 2010; 101(8):1828–33. [PubMed: 20545695]
30. Chen WC, Hsu HP, Li CY, Yang YJ, Hung YH, Cho CY, Wang CY, Weng TY, Lai MD. Cancer stem cell marker CD90 inhibits ovarian cancer formation via beta3 integrin. International journal of oncology. 2016; 49(5):1881–1889. [PubMed: 27633757]
31. Carduner L, Picot CR, Leroy-Dudal J, Blay L, Kellouche S, Carreiras F. Cell cycle arrest or survival signaling through alphav integrins, activation of PKC and ERK1/2 lead to anoikis resistance of ovarian cancer spheroids. Exp Cell Res. 2014; 320(2):329–42. [PubMed: 24291221]
32. Shi J, Jin Z, Liu X, Fan D, Sun Y, Zhao H, Zhu Z, Liu Z, Jia B, Wang F. PET imaging of neovascularization with (68)Ga-3PRGD2 for assessing tumor early response to Endostar antiangiogenic therapy. Molecular pharmaceutics. 2014; 11(11):3915–22. [PubMed: 25158145]

33. Hernandez R, Valdovinos HF, Yang Y, Chakravarty R, Hong H, Barnhart TE, Cai W. (44)Sc: an attractive isotope for peptide-based PET imaging. Molecular pharmaceutics. 2014; 11(8):2954–61. [PubMed: 25054618]
34. Hu H, Li D, Liu S, Wang M, Moats R, Conti PS, Li Z. Integrin alpha2beta1 targeted GdVO4:Eu ultrathin nanosheet for multimodal PET/MR imaging. Biomaterials. 2014; 35(30):8649–58. [PubMed: 25043573]
35. Tan M, Lu ZR. Integrin Targeted MR Imaging. Theranostics. 2011; 1:83–101. [PubMed: 21547154]
36. Yoon HY, Shin ML, Shim MK, Lee S, Na JH, Koo H, Lee H, Kim JH, Lee KY, Kim K, Kwon IC. Artificial Chemical Reporter Targeting Strategy Using Bioorthogonal Click Reaction for Improving Active-Targeting Efficiency of Tumor. Molecular pharmaceutics. 2017; 14(5):1558–1570. [PubMed: 28191852]
37. Chen Y, Feng S, Liu W, Yuan Z, Yin P, Gao F. Vitamin E Succinate-Grafted-Chitosan Oligosaccharide/RGD-Conjugated TPGS Mixed Micelles Loaded with Paclitaxel for U87MG Tumor Therapy. Molecular pharmaceutics. 2017; 14(4):1190–1203. [PubMed: 28212490]
38. Chen L, Liu Y, Wang W, Liu K. Effect of integrin receptor-targeted liposomal paclitaxel for hepatocellular carcinoma targeting and therapy. Oncol Lett. 2015; 10(1):77–84. [PubMed: 26170980]
39. Xiao D, Jia HZ, Ma N, Zhuo RX, Zhang XZ. A redox-responsive mesoporous silica nanoparticle capped with amphiphilic peptides by self-assembly for cancer targeting drug delivery. Nanoscale. 2015; 7(22):10071–7. [PubMed: 25978679]
40. Malamas AS, Jin E, Gujrati M, Lu ZR. Dynamic Contrast Enhanced MRI Assessing the Antiangiogenic Effect of Silencing HIF-1alpha with Targeted Multifunctional ECO/siRNA Nanoparticles. Molecular pharmaceutics. 2016; 13(7):2497–506. [PubMed: 27264671]
41. Minchinton AI, Tannock IF. Drug penetration in solid tumours. Nature reviews Cancer. 2006; 6(8): 583–92. [PubMed: 16862189]
42. Huang L, Sullenger B, Juliano R. The role of carrier size in the pharmacodynamics of antisense and siRNA oligonucleotides. J Drug Target. 2010; 18(8):567–74. [PubMed: 20367081]
43. Matsumura Y, Maeda H. A new concept for macromolecular therapeutics in cancer chemotherapy: mechanism of tumoritropic accumulation of proteins and the antitumor agent smancs. Cancer research. 1986; 46(12 Pt 1):6387–92. [PubMed: 2946403]
44. Ruenraroengsak P, Cook JM, Florence AT. Nanosystem drug targeting: Facing up to complex realities. Journal of controlled release : official journal of the Controlled Release Society. 2010; 141(3):265–76. [PubMed: 19895862]
45. Chauhan VP, Stylianopoulos T, Boucher Y, Jain RK. Delivery of molecular and nanoscale medicine to tumors: transport barriers and strategies. Annual review of chemical and biomolecular engineering. 2011; 2:281–98.
46. Heldin CH, Rubin K, Pietras K, Ostman A. High interstitial fluid pressure - an obstacle in cancer therapy. Nature reviews Cancer. 2004; 4(10):806–13. [PubMed: 15510161]
47. Siegel RL, Miller KD, Jemal A. Cancer statistics, 2016. CA: a cancer journal for clinicians. 2016; 66(1):7–30. [PubMed: 26742998]
48. Hennessy BT, Coleman RL, Markman M. Ovarian cancer. Lancet. 2009; 374(9698):1371–82. [PubMed: 19793610]
49. Lengyel E. Ovarian cancer development and metastasis. The American journal of pathology. 2010; 177(3):1053–64. [PubMed: 20651229]
50. Cannistra SA, Ottensmeier C, Niloff J, Orta B, DiCarlo J. Expression and function of beta 1 and alpha v beta 3 integrins in ovarian cancer. Gynecologic oncology. 1995; 58(2):216–25. [PubMed: 7542622]
51. Liapis H, Adler LM, Wick MR, Rader JS. Expression of alpha(v)beta3 integrin is less frequent in ovarian epithelial tumors of low malignant potential in contrast to ovarian carcinomas. Human pathology. 1997; 28(4):443–9. [PubMed: 9104944]
52. Yuan A, Yang B, Wu J, Hu Y, Ming X. Dendritic nanoconjugates of photosensitizer for targeted photodynamic therapy. Acta biomaterialia. 2015; 21:63–73. [PubMed: 25900441]

53. Ming X, Carver K, Wu L. Albumin-based nanoconjugates for targeted delivery of therapeutic oligonucleotides. Biomaterials. 2013; 34(32):7939–49. [PubMed: 23876758]
54. Herre J, Marshall AS, Caron E, Edwards AD, Williams DL, Schweighoffer E, Tybulewicz V, Reis e Sousa C, Gordon S, Brown GD. Dectin-1 uses novel mechanisms for yeast phagocytosis in macrophages. Blood. 2004; 104(13):4038–45. [PubMed: 15304394]
55. Uriarte SM, Jog NR, Luerman GC, Bhimani S, Ward RA, McLeish KR. Counterregulation of clathrin-mediated endocytosis by the actin and microtubular cytoskeleton in human neutrophils. Am J Physiol Cell Physiol. 2009; 296(4):C857–67. [PubMed: 19176760]
56. Groppelli E, Tuthill TJ, Rowlands DJ. Cell entry of the aphthovirus equine rhinitis A virus is dependent on endosome acidification. J Virol. 2010; 84(12):6235–40. [PubMed: 20375159]
57. Chang CC, Wu M, Yuan F. Role of specific endocytic pathways in electrotransfection of cells. Mol Ther Methods Clin Dev. 2014; 1:14058. [PubMed: 26052524]
58. Robinson MS. The role of clathrin, adaptors and dynamin in endocytosis. Current opinion in cell biology. 1994; 6(4):538–44. [PubMed: 7986531]
59. Ming X, Sato K, Juliano RL. Unconventional internalization mechanisms underlying functional delivery of antisense oligonucleotides via cationic lipoplexes and polyplexes. J Control Release. 2011; 153(1):83–92. [PubMed: 21571016]
60. Ming X, Alam MR, Fisher M, Yan Y, Chen X, Juliano RL. Intracellular delivery of an antisense oligonucleotide via endocytosis of a G protein-coupled receptor. Nucleic Acids Res. 2010; 38(19): 6567–76. [PubMed: 20551131]
61. Khalil IA, Kogure K, Akita H, Harashima H. Uptake pathways and subsequent intracellular trafficking in nonviral gene delivery. Pharmacol Rev. 2006; 58(1):32–45. [PubMed: 16507881]
62. Caswell PT, Norman JC. Integrin trafficking and the control of cell migration. Traffic. 2006; 7(1): 14–21. [PubMed: 16445683]
63. Muro S. Challenges in design and characterization of ligand-targeted drug delivery systems. Journal of controlled release : official journal of the Controlled Release Society. 2012; 164(2):125–37. [PubMed: 22709588]
64. Montet X, Funovics M, Montet-Abou K, Weissleder R, Josephson L. Multivalent effects of RGD peptides obtained by nanoparticle display. J Med Chem. 2006; 49(20):6087–93. [PubMed: 17004722]
65. Johansson S, Svineng G, Wennerberg K, Armulik A, Lohikangas L. Fibronectin-integrin interactions. Front Biosci. 1997; 2:d126–46. [PubMed: 9159220]
66. De Nichilo MO, Burns GF. Granulocyte-macrophage and macrophage colony-stimulating factors differentially regulate alpha v integrin expression on cultured human macrophages. Proceedings of the National Academy of Sciences of the United States of America. 1993; 90(6):2517–21. [PubMed: 7681600]
67. Ammon C, Meyer SP, Schwarzfischer L, Krause SW, Andreesen R, Kreutz M. Comparative analysis of integrin expression on monocyte-derived macrophages and monocyte-derived dendritic cells. Immunology. 2000; 100(3):364–9. [PubMed: 10929059]
68. Cui Y, Guo G. Immunomodulatory Function of the Tumor Suppressor p53 in Host Immune Response and the Tumor Microenvironment. Int J Mol Sci. 2016; 17(11)
69. Gabrilovich DI, Ostrand-Rosenberg S, Bronte V. Coordinated regulation of myeloid cells by tumours. Nat Rev Immunol. 2012; 12(4):253–68. [PubMed: 22437938]
70. Brady NJ, Chuntova P, Schwertfeger KL. Macrophages: Regulators of the Inflammatory Microenvironment during Mammary Gland Development and Breast Cancer. Mediators Inflamm. 2016; 2016:4549676. [PubMed: 26884646]
71. Veglia F, Gabrilovich DI. Dendritic cells in cancer: the role revisited. Curr Opin Immunol. 2017; 45:43–51. [PubMed: 28192720]
72. Friedrich J, Seidel C, Ebner R, Kunz-Schughart LA. Spheroid-based drug screen: considerations and practical approach. Nature protocols. 2009; 4(3):309–24. [PubMed: 19214182]
73. Mehta G, Hsiao AY, Ingram M, Luker GD, Takayama S. Opportunities and challenges for use of tumor spheroids as models to test drug delivery and efficacy. Journal of controlled release : official journal of the Controlled Release Society. 2012; 164(2):192–204. [PubMed: 22613880]

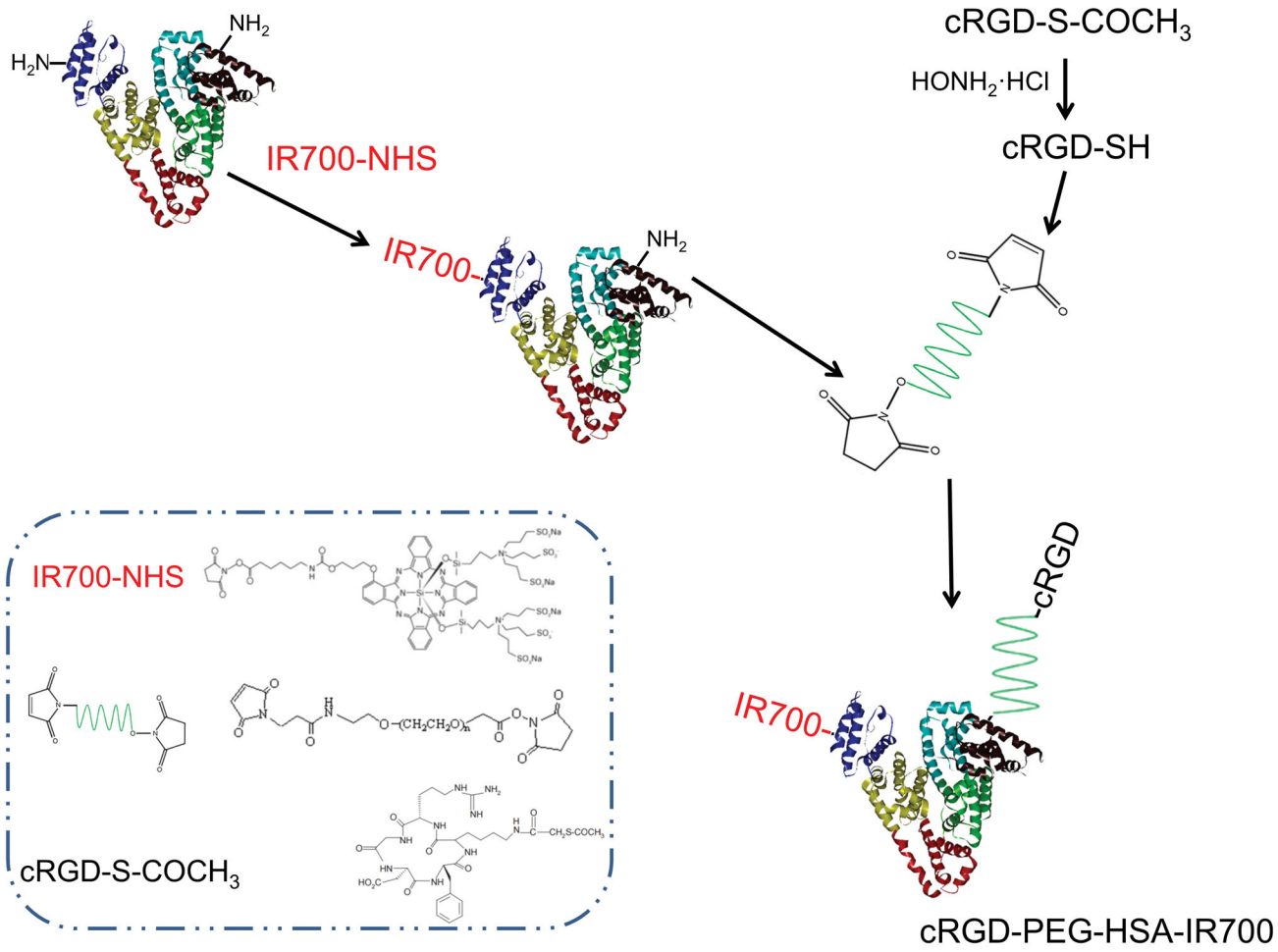

Fig. 1.
Synthesis scheme of the targeted cRGD-PEG-HSA-IR700 nanoconjugates.

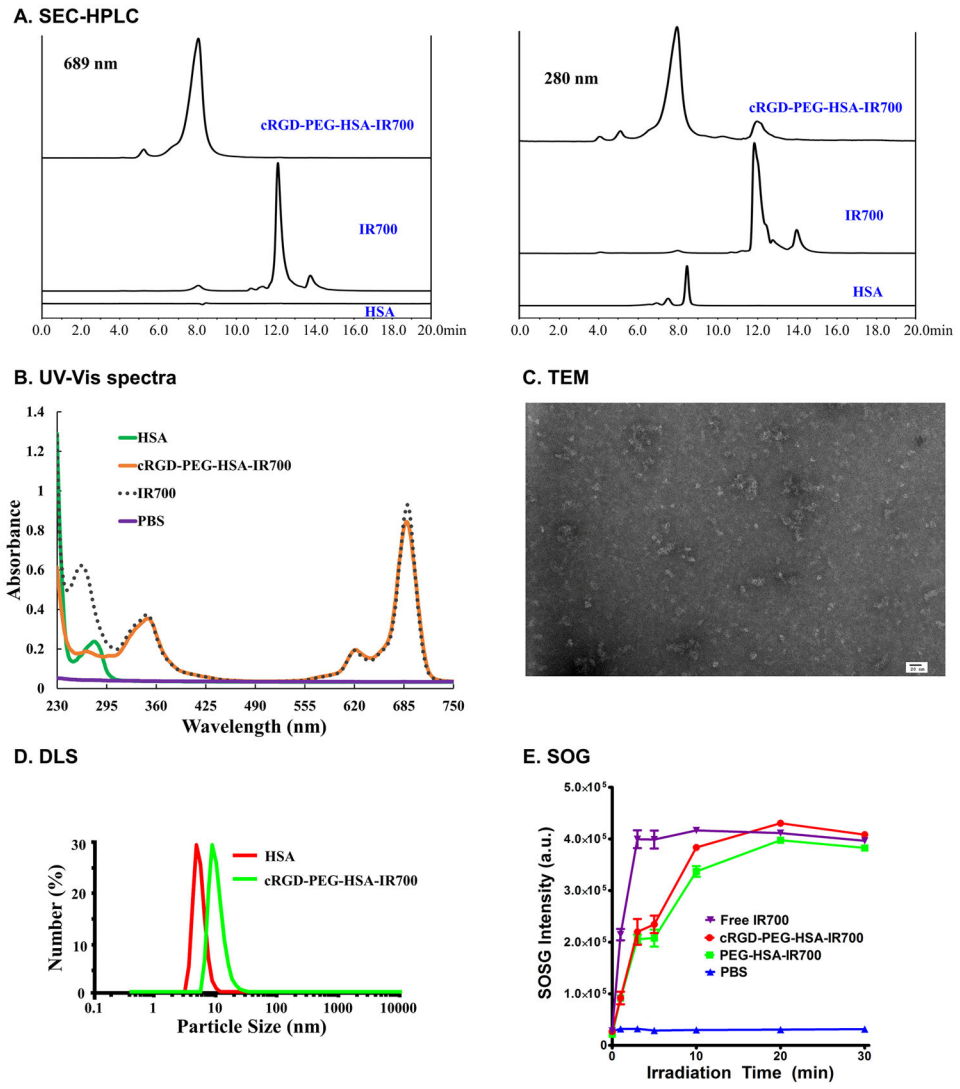

Fig. 2.

Characterization of the targeted nanoconjugates. A. SEC-HPLC chromatography of cRGD-PEG-HSA-IR700, IR700, and HSA (left: λ = 689 nm; right: λ = 280 nm). B. The UV-Vis absorbance spectra of PBS, HSA, free IR700, and cRGD-PEG-HSA-IR700. C. TEM image of the cRGD-PEG-HSA-IR700 nanoconjugates. The average particle size was estimated to be 10 nm. D. Particle size distribution of HSA and cRGD-PEG-HSA-IR700 determined by DLS. E. Time-dependent singlet oxygen generation of PBS, free IR700, PEG-HSA-IR700 and cRGD-PEG-HSA-IR700.

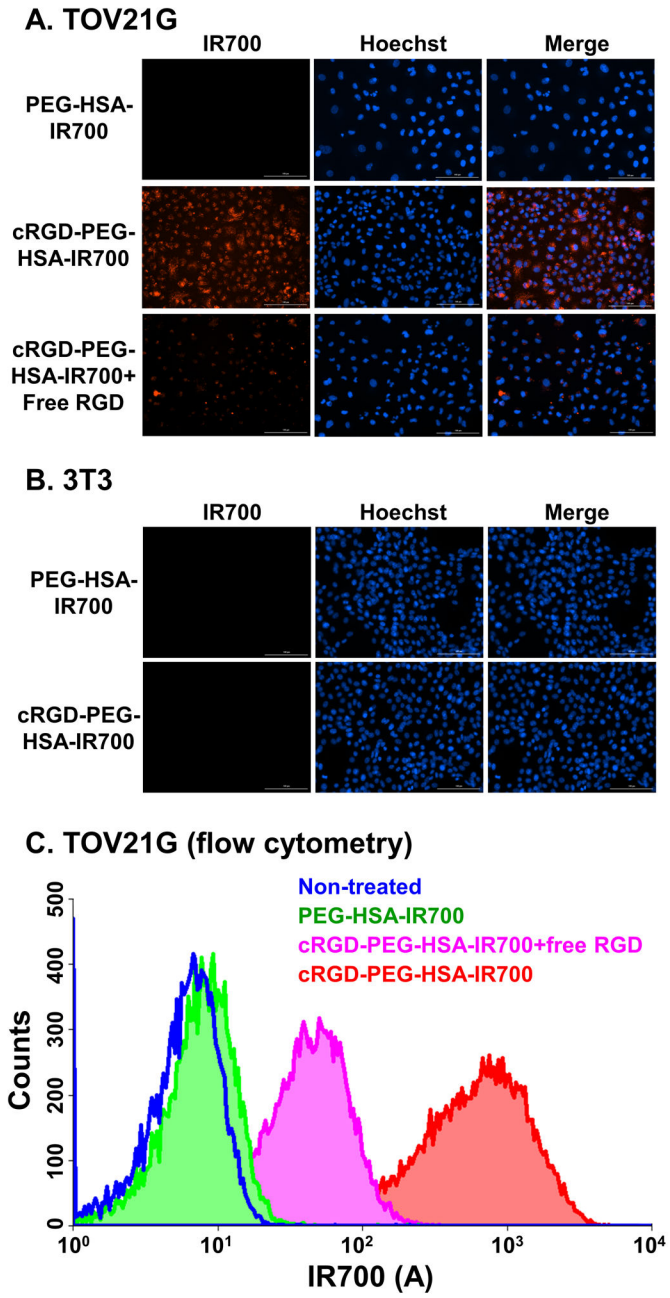

Fig. 3.

Intracellular uptake of the nanoconjugates. A. Fluorescent images of cellular uptake of PEG-HSA-IR700 and cRGD-PEG-HSA-IR700 nanoconjugates in the absence and presence of free RGD peptide in TOV21G cells. B. Fluorescent images of cellular uptake of PEG-HSA-IR700 and cRGD-PEG-HSA-IR700 nanoconjugates in NIH/3T3 cells. C. Flow cytometry histogram for cellular uptake of PEG-HSA-IR700 and cRGD-PEG-HSA-IR700 nanoconjugates in the absence and presence of free RGD peptide in TOV21G cells.

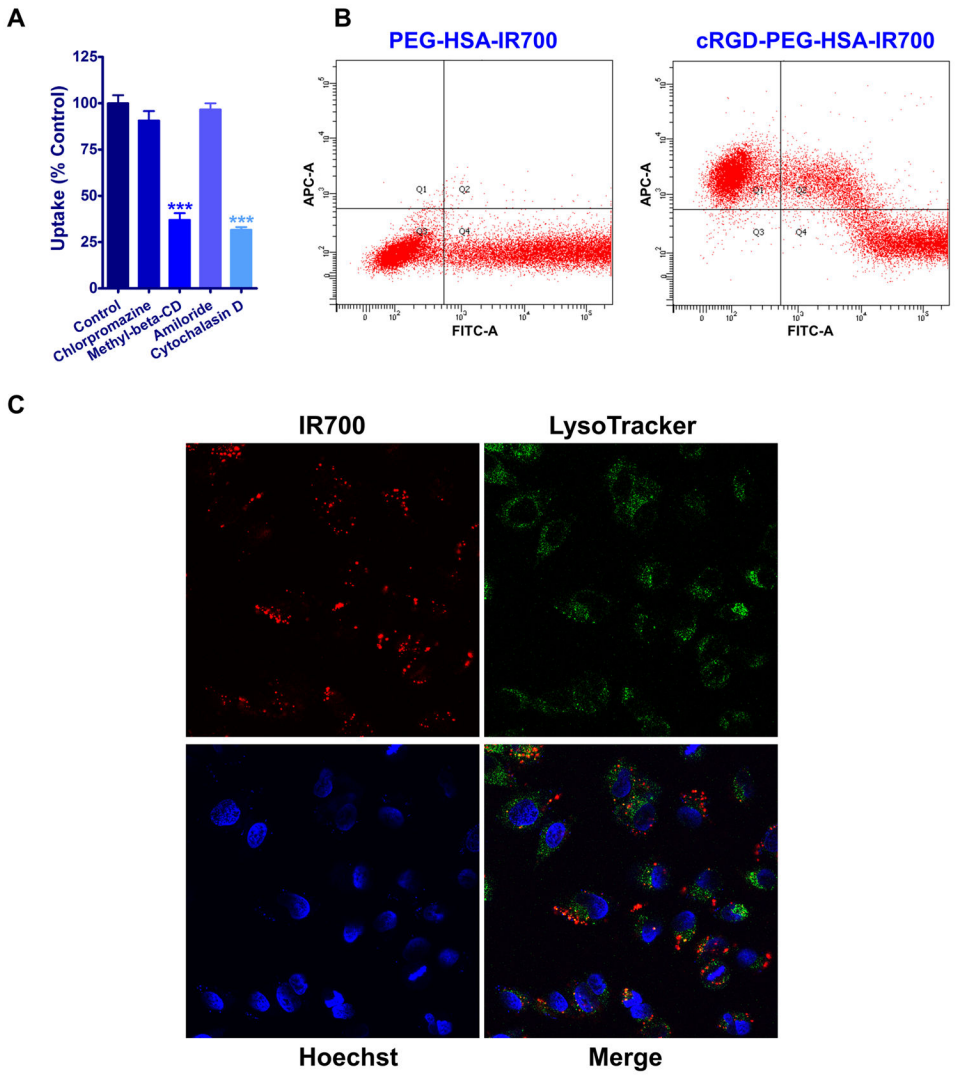

Fig. 4.

Intracellular uptake pathway of the targeted nanoconjugates. A. Effects of endocytosis inhibitors on the cRGD-PEG-HSA-IR700 uptake in TOV21G cells were evaluated with flow cytometry. B. Effects of dominant negative dynamin on cellular uptake of PEG-HSA-IR700 and cRGD-PEG-HSA-IR700 in TOV21G cells were examined using flow cytometry. C. Co-localization of Lysotracker Green with the cRGD-PEG-HSA-IR700 nanoconjugates in TOV21G cells was observed using confocal microscopy.

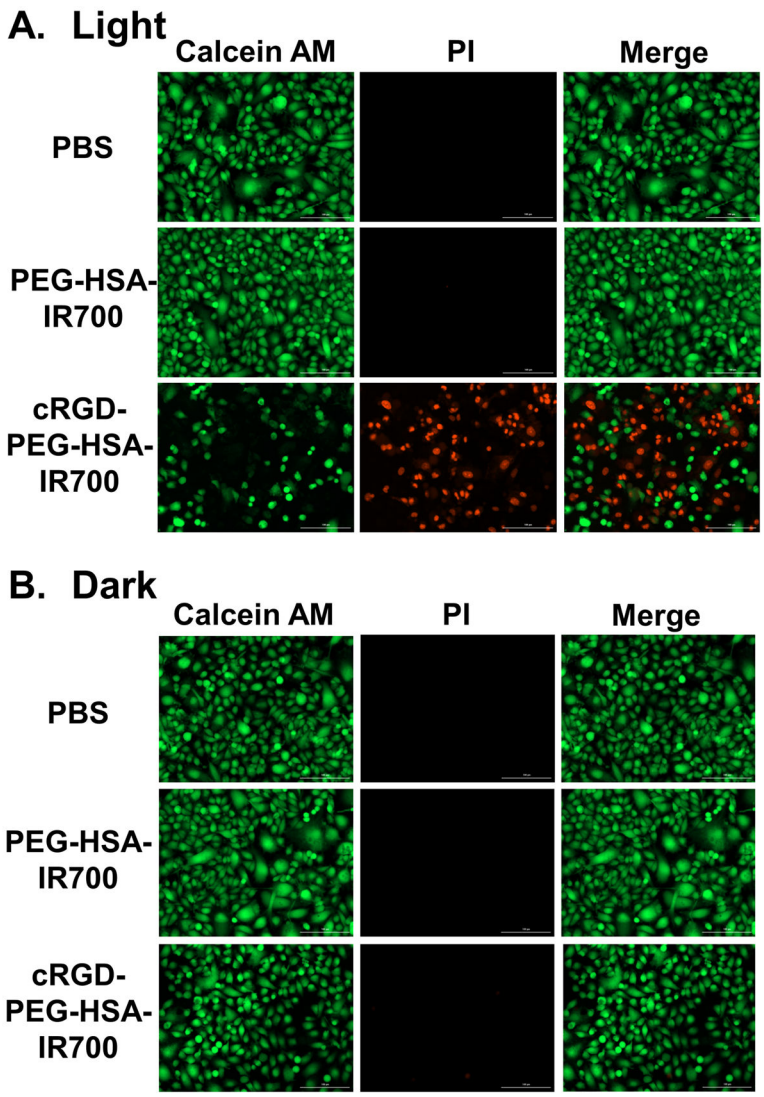

Fig. 5.

Live/dead staining of TOV21G cells after targeted PDT. TOV21G cells were treated with the PEG-HSA-IR700 or cRGD-PEG-HSA-IR700 nanoconjugates overnight. Live/dead staining was performed after some cells were irradiated with a 660 nm LED light (A), and the others were not (B).

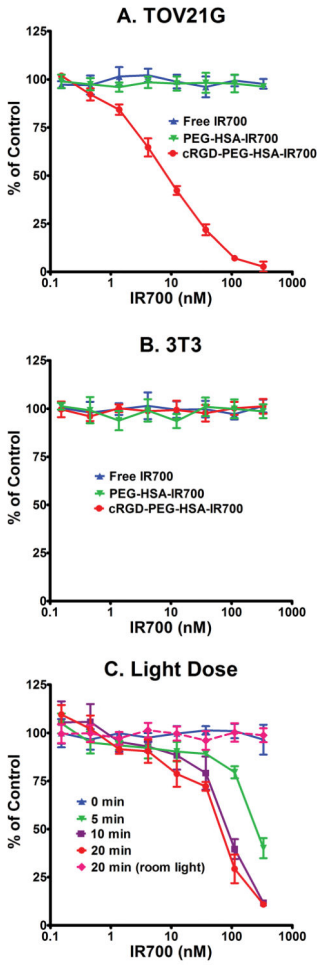

Fig. 6.

Dose- and light-dependent cytotoxicity of nanoconjugates. A. Dose-dependent phototoxicity in TOV21G cells. Alamar Blue assay was performed after PDT of TOV21G with free IR700, PEG-HSA-IR700 and cRGD-PEG-HSA-IR700 (n = 4). B. Dose-dependent phototoxicity in NIH/3T3 cells (n = 4). C. light dose-dependent cytotoxicity of nanoconjugates. The effect of light dose on photokilling of cRGD-PEG-HSA-IR700 was examined in TOV21G cells using Alamar Blue assay (n = 4).

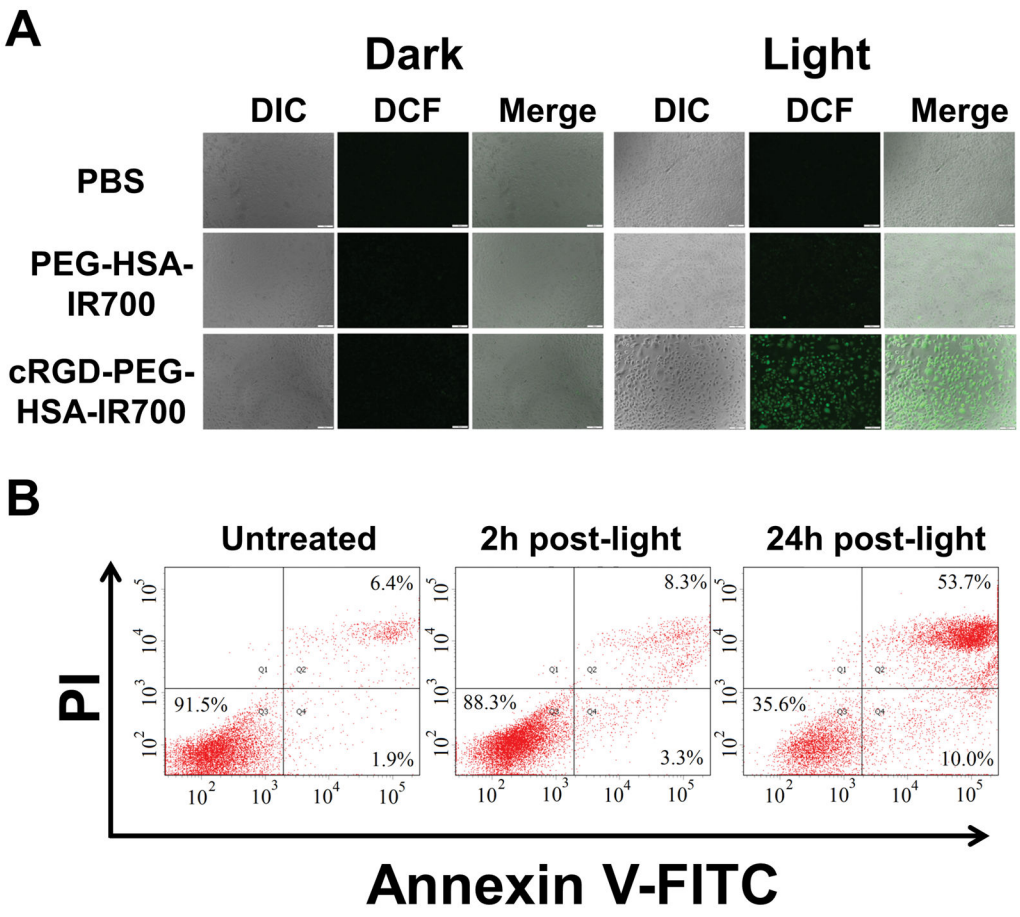

Fig. 7.

Mechanisms of targeted PDT. A. Intracellular singlet oxygen detection. Fluorescence images of ROS generation were taken after PDT in TOV21G cells. B. Flow cytometric analysis of apoptosis in TOV21G cells after cRGD-PEG-HSA-IR700 mediated PDT.

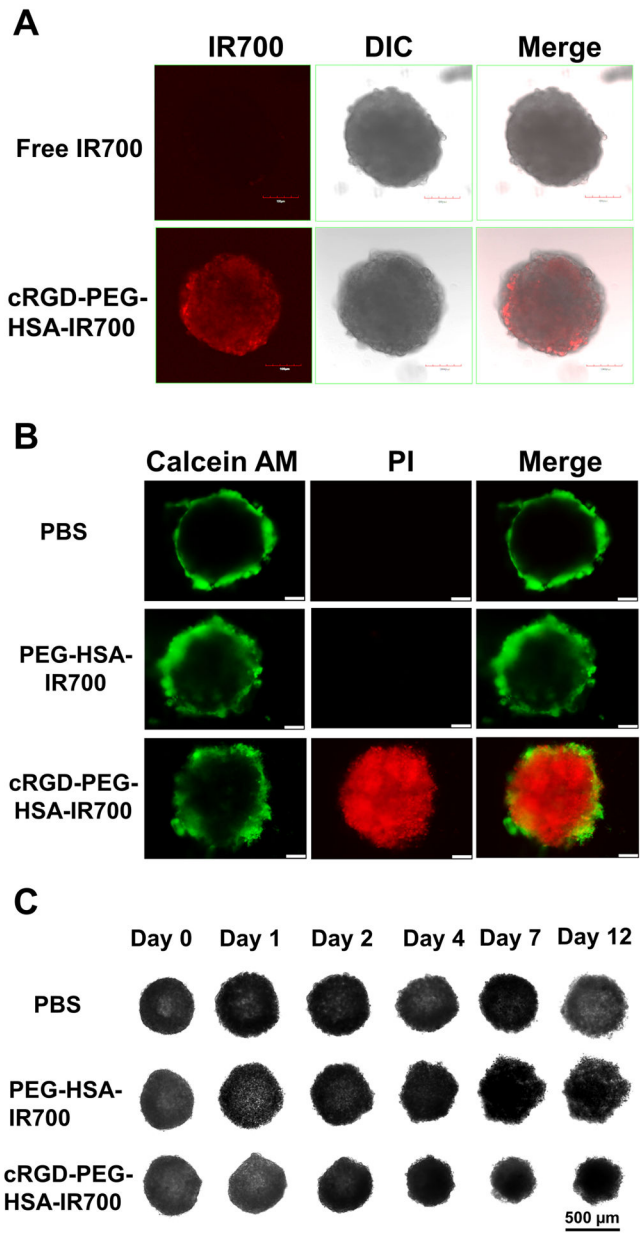

Fig. 8.

Penetration and phototoxicity of cRGD-PEG-HSA-IR700 nanoconjugates in SKOV-3 spheroids. A. Penetration of the targeted nanoconjugates in tumor spheroids. Tumor spheroids of SKOV-3 cells were treated with free IR700 or cRGD-PEG-HSA-IR700 nanoconjugates for 4 h. After washing, the spheroids were observed by confocal microscopy. B. Live/dead staining of SKOV-3 spheroids after photokilling of the nanoconjugates. SKOV-3 spheroids were treated with PEG-HSA-IR700 or cRGD-PEG-HSA-IR700 nanoconjugates overnight. After washing, the spheroids were irradiated with the 660 nm LED light. Live/dead staining of SKOV-3 spheroids was performed after 24 h. C. Growth of SKOV-3 spheroids after photokilling of the nanoconjugates. After photokilling, the growth

of spheroids was monitored by using a CYTATION 5 imaging reader over the following 12 days.